Experimental and Theoretical Studies of Double Minima in the Potential-Energy Surfaces for HF-Elimination Reactions of $SiF_x(OH)_y^+$ with H_2O ($x = 1-3$, $y = 0-2$) via Intramolecular H-Atom Transfer

A. E. Ketvirtis, V. I. Baranov, A. C. Hopkinson,* and D. K. Bohme*

Department of Chemistry and Centre for Research in Earth and Space Science, York University, North York, Ontario, Canada M3J 1P3

Received: October 9, 1997; In Final Form: December 1, 1997

HF elimination reactions between H_2O and ions of the type $SiF_x(OH)_y^+$ with ($x = 1-3$, $y = 0-2$) have been observed and are shown by computation to proceed by intramolecular H-atom transfer on potential-energy surfaces characterized by double minima. The chemistry was initiated by SiF^+, $SiF_2^{\bullet+}$ and SiF_3^+ in H_2O using the selected-ion flow tube (SIFT) technique at 293 ± 4 K in helium buffer gas at 0.35 ± 0.01 Torr. All three cations were observed to react with H_2O by sequential HF elimination until all Si−F bonds in these cations were replaced by Si−O bonds in agreement, in the case of the chemistry initiated by SiF_3^+, with previous low-pressure FT-ICR measurements by Speranza *et al.* $SiOH^+$ does not react further with water, but the terminal $Si(OH)_2^{\bullet+}$ ion in the sequence initiated by $SiF_2^{\bullet+}$ reacts further with H_2O by H-atom elimination (90%) and H_2O addition (10%), while $Si(OH)_3^+$, the terminal ion in the sequence initiated by SiF_3^+, was observed to sequentially add two water molecules under SIFT conditions. Products and rate coefficients were measured for all primary and higher-order reactions. For closed-shell species gradient structure optimizations and harmonic frequency calculations were performed on critical points at HF/3-21G and with density functional theory using B-LYP/6-31G(d,p); reactants and products for open-shell species were examined at ROHF/3-21G and at ROHF/6-31G(d,p). On all the potential-energy surfaces studied, the hydrogen fluoride elimination pathway was shown to proceed through a hydrated reactant ion and an HF-solvated product ion, each at local minima, separated by a transition structure for H-atom transfer; the energies of these three critical points, in all cases, lie below those of the reactants and of the products. The measured HF-elimination efficiency increases with increasing energy defect between the initial reactants and the transition state.

Introduction

It is well-established that bonding between silicon and fluorine is very strong.[1] Of course silicon also forms strong bonds with oxygen,[1] and the chemical literature is replete with theoretical[2] and experimental gas-phase[3,4] studies of Si−O bonding. Si−O bonds generally are weaker (ca. 108 kcal mol^{-1})[1] than Si−F bonds (ca. 135 kcal mol^{-1}),[1] but exothermic ion−molecule reactions are known in which a stronger bond is replaced by a weaker one. This is clearly evident, for example, in the reaction of SiF_3^+ with H_2O, which has been shown in recent low-pressure FT-ICR experiments[4] to react rapidly in the gas phase by HF-elimination, reaction 1, for which the driving force is provided

$$SiF_3^+ + H_2O \rightarrow SiF_2OH^+ + HF \qquad (1)$$

by the greater strength of the F−H bond (136 kcal mol^{-1})[5] formed in the products compared to that of the HO−H bond broken (119 kcal mol^{-1}).[6] Indeed, this force continues to efficently drive further sequential bond transformations of this type, according to reactions 2 and 3, until all Si−F bonds have

$$SiF_2OH^+ + H_2O \rightarrow SiF(OH)_2^+ + HF \qquad (2)$$

$$SiF(OH)_2^+ + H_2O \rightarrow Si(OH)_3^+ + HF \qquad (3)$$

been exchanged for Si−OH bonds by HF elimination.[4] Here we explore further such bond transformations both experimentally and theoretically. The kinetics of reactions 1−3, together with the related reactions of $SiF_2^{\bullet+}$ and SiF^+ with H_2O, were investigated systematically with the substantially higher-pressure selected-ion flow tube (SIFT) technique. Also, molecular orbital calculations were performed for the ions observed experimentally, as well as for plausible intermediates and transition states. These have provided insights into details of the relevant potential-energy surfaces from which have emerged a mechanism common to all of the observed HF-elimination reactions of SiF^+, $SiF_2^{\bullet+}$, $SiFOH^{\bullet+}$, SiF_3^+, SiF_2OH^+, and $SiF(OH)_2^+$ with H_2O, viz., reactions of type (4) for ($x = 1-3$, $y = 0-2$). This mechanism involves H-atom transfer on a double-minimum potential-energy surface and accounts for the observed trends in reaction kinetics.

$$SiF_x(OH)_y^+ + H_2O \rightarrow SiF_{x-1}(OH)_{y+1}^+ + HF \qquad (4)$$

Experimental Method

The gas-phase ion−molecule reactions reported in this study were investigated with the SIFT technique in the Ion Chemistry Laboratory at York University, a technique that has been described previously in the literature.[7,8] The SiF_n^+ ions were produced by electron impact upon neutral SiF_4 (Matheson, > 99.6 mol %) in a low-pressure ion source from a 3% mixture of SiF_4 in helium at various electron energies: 50 eV for SiF_3^+,

S1089-5639(97)03287-8 CCC: $15.00
Published on Web 01/27/1998

70 eV for $SiF_2^{\bullet+}$, and 80 eV for SiF^+. They were then mass-selected with a quadrupole mass filter and introduced via a Venturi inlet into a flow of helium buffer gas at a pressure of 0.35 Torr. H_2O was added into the reaction region downstream as a vapor diluted with helium. Reactant and product ions were followed as a function of the amount of added vapor. Rate coefficients were determined in the usual manner.[7,8]

The rate coefficients for primary reactions reported here are estimated to have an uncertainty of ±30%. Higher-order rate coefficients were obtained by fitting the experimental data to the solutions of the system of differential equations for successive reactions. Reverse reactions were not included. The one branching reaction observed was included explicitly in the reaction mechanism. The accuracy for this fitting procedure depends on several parameters and is reported separately for every calculated high-order rate coefficient.

Computational Methods

Theoretical calculations were performed using the GAUSSIAN suite of programs.[9] Geometric optimizations of all structures at critical points on closed-shell potential-energy surfaces have been performed with the restricted Hartree−Fock (RHF) formalism with a split-valence 3-21G basis set.[10] Subsequently, geometric optimizations were performed on the same molecules with the density fuctional[11] Becke technique, which includes the Slater (local spin density) exchange functional[11a,b,12] with nonlocal gradient-corrected terms included,[13] and the Lee−Yang−Parr method, which includes local and nonlocal gradient-corrected correlation functionals.[14] Structure optimizations and subsequent harmonic frequency calculations at this level (henceforth denoted B-LYP) were performed using the standard Gaussian split-valence 6-31G(d,p) basis set.[14,15] Transition structures were located either by an initial point-by-point profile analysis, followed by refinement with the eigenvector-following (EF) algorithm,[16] or by direct calculations from the geometries of the two associated local minima by the synchronous transit-guided quasi-Newton (STQN) method.[17] Intrinsic reaction coordinate (IRC)[18] analyses were performed to verify the identities of the two ions at local minima which are interconnected through each transition structure. All critical points on the potential energy hypersurfaces were characterized by harmonic frequency calculations at the same level of theory; these calculations also yielded zero-point vibrational energies. At this level of theory, we estimate conservatively that the error in relative energies will be $<\pm 5$ kcal mol^{-1}, although this particular type of calculation has not been widely used.

Geometric optimizations of all critical points on open-shell potential-energy surfaces have been performed with the restricted open-shell Hartree−Fock (ROHF)[19] formalism, first with a 3-21G basis set and then with a 6-31G(d,p) basis set. Harmonic frequency calculations were performed at ROHF/6-31G(d,p) on all critical points optimized at this level of theory.

Results and Discussion

Reaction Kinetics. Figures 1−3 show experimental results obtained for the ion chemistry initiated by the reactions of SiF^+, $SiF_2^{\bullet+}$, and SiF_3^+ with H_2O under SIFT conditions of 0.35 ± 0.01 Torr of helium and at 294 ± 3 K. The rate coefficients for the three primary reactions obtained from the semilogarithmic decays of the primary ions are summarized in Table 1 and the higher-order kinetics obtained by fitting observed signal profiles for the higher order ions is surveyed in Table 2.

Figure 1 shows that SiF^+ reacts relatively slowly, $k = 7.6 \times 10^{-11}$ cm^3 $molecule^{-1}$ s^{-1}, with a low efficiency, 0.030 (see Table 1), according to the HF-elimination reaction 5. No further reaction of $SiOH^+$ with H_2O was observed in the flow range shown.

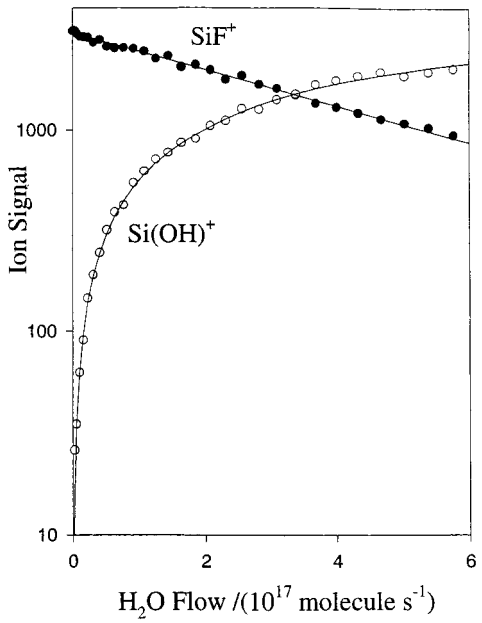

Figure 1. Measured profiles for the reaction of SiF^+ with added water vapor. The solid lines represent fits of the data to solutions of the appropriate differential equations.

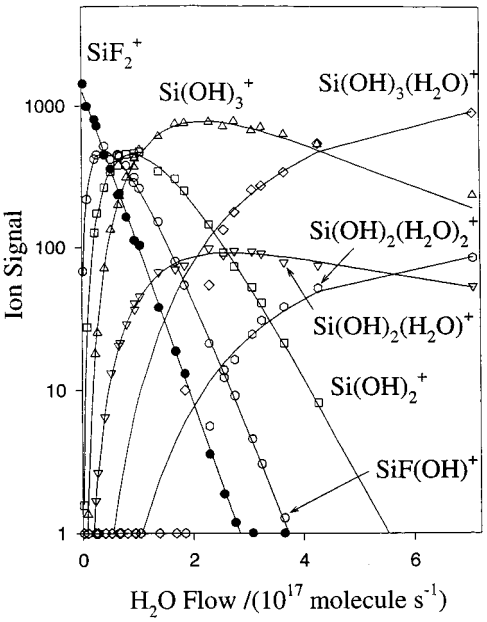

Figure 2. Measured profiles for the reactions initiated by $SiF_2^{\bullet+}$ in added water vapor. The solid lines represent fits of the data to solutions of the appropriate differential equations.

$$SiF^+ + H_2O \rightarrow SiOH^+ + HF \qquad (5)$$

The water chemistry observed with $SiF_2^{\bullet+}$ is shown in Figure 2 and is much more extensive than that observed with SiF^+. The two sequential HF elimination reactions 6 and 7 quickly

$$SiF_2^{\bullet+} + H_2O \rightarrow SiF(OH)^{\bullet+} + HF \qquad (6)$$

$$SiF(OH)^{\bullet+} + H_2O \rightarrow Si(OH)_2^{\bullet+} + HF \qquad (7)$$

establish two Si−OH bonds at the expense of the two Si−F

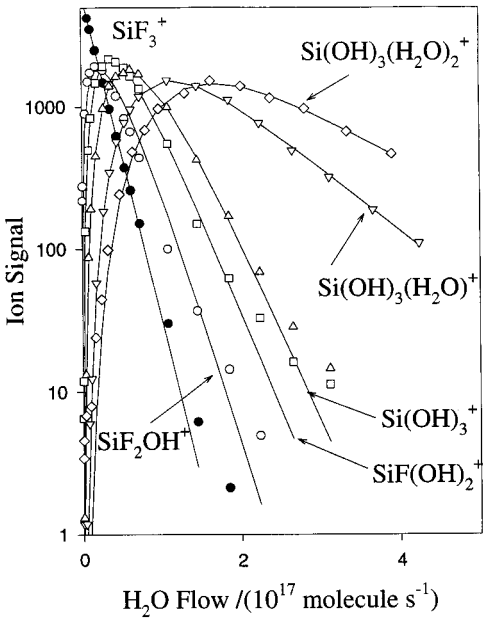

Figure 3. Measured profiles for the reactions initiated by SiF_3^+ in added water vapor. The solid lines represent fits of the data to solutions of the appropriate differential equations. Not shown is the primary F-elimination channel leading to the formation of $SiF_2OH_2^{\bullet+}$ and the ensuing HF-elimination chemistry of this ion (see text).

TABLE 1: Rate Coefficients, Product Distributions, and Reaction Efficiencies for the Primary Reactions of SiF_x^+ ($x = 1-3$) with H_2O

reactant ion	products	product distribution[a]	k_{exp}[b]	k_c[c]	k_{exp}/k_c[d]
SiF^+	$SiOH^+ + HF$	1.0	0.76	25	0.030
SiF_2^+	$SiFOH^+ + HF$	1.0	9.3	24	0.39
SiF_3^+	$SiF_2OH^+ + HF$	1.0	16	23	0.70

[a] Product distributions have been rounded to the nearest 5%. [b] Effective bimolecular rate coefficients in units of 10^{-10} cm^3 molecule^{-1} s^{-1} measured at a temperature of 294 ± 3 K and at a helium buffer gas pressure of 0.35 ± 0.01 Torr. Absolute accuracies are estimated to be less than $\pm 30\%$; relative accuracies are smaller than $\pm 10\%$. [c] Collision rate coefficients in units of 10^{-10} cm^3 molecule^{-1} s^{-1} derived from a variational transition-state treatment.[22] [d] k_{exp}/k_c is a measure of reaction efficiency.

bonds in $SiF_2^{\bullet+}$. Interestingly, the $Si(OH)_2^{\bullet+}$ produced in reaction 7 reacts further with H_2O in a reasonably fast reaction, $k = 5.8 \times 10^{-10}$ cm^3 molecule^{-1} s^{-1}, primarily (90%) by H-atom elimination to establish $Si(OH)_3^+$. This bimolecular channel competes with hydration (10%) as shown in reaction 8. Hydration presumably occurs in a termolecular fashion under

$$Si(OH)_2^{\bullet+} + H_2O \rightarrow Si(OH)_3^+ + H^{\bullet} \quad (8a)$$

$$\rightarrow Si(OH)_2(H_2O)^{\bullet+} \quad (8b)$$

our experimental operating conditions, but radiative association cannot be ruled out since the reaction was not investigated as a function of pressure. Both $Si(OH)_3^+$ and $Si(OH)_2(H_2O)^+$ were observed to add one more water molecule in the flow range investigated according to reactions 9 and 10.

$$Si(OH)_3^+ + H_2O \rightarrow Si(OH)_3(H_2O)^+ \quad (9)$$

$$Si(OH)_2(H_2O)^{\bullet+} + H_2O \rightarrow Si(OH)_2(H_2O)_2^{\bullet+} \quad (10)$$

Results obtained for the reaction of SiF_3^+ with water are shown in Figure 3. The sequential bond redisposition indicated

TABLE 2: Rate Coefficients, Product Distributions, and Reaction Efficiencies for Secondary and Higher-Order Reactions Initiated by SiF_x^+ ($x = 1-3$) Reacting with H_2O

reactant ion	products	product distribution[a]	k_{exp}[b]	k_c[c]	k_{exp}/k_c[d]
		Secondary Reactions			
$SiFOH^+$	$SiO_2H_2^+ + HF$	1.0	9.3	23	0.40
SiF_2OH^+	$SiFO_2H_2^+ + HF$	1.0	11	23	0.48
		Tertiary Reactions			
$SiO_2H_2^+$	$SiO_3H_3^+ + H$	0.9	5.8	24	0.24
	$SiO_3H_4^+$	0.1			
$SiFO_2H_2^+$	$SiO_3H_3^+ + HF$	1.0	8.5	23	0.37
		Quaternary Reactions			
$SiO_3H_3^+$	$SiO_4H_5^+$	1.0	1.0[e]	23	0.043
			7.7[f]	23	0.33
$SiO_3H_4^+$	$SiO_4H_6^+$	1.0	0.45	23	0.020
		Quinary Reaction			
$SiO_4H_5^+$	$SiO_5H_7^+$	1.0	3.2	23	0.14

[a] Product distributions have been rounded to the nearest 5%. [b] Effective bimolecular rate coefficients in units of 10^{-10} cm^3 molecule^{-1} s^{-1} measured at a temperature of 294 ± 3 K and at a helium buffer gas pressure of 0.35 ± 0.01 Torr. Absolute accuracies are estimated to be less than $\pm 30\%$ for primary and secondary reactions and less than $\pm 50\%$ for the higher-order reactions. [c] Collision rate coefficients in units of 10^{-10} cm^3 molecule^{-1} s^{-1} derived from a variational transition-state treatment.[22] [d] k_{exp}/k_c is a measure of reaction efficiency. [e] $SiO_3H_3^+$ produced from the reaction of $Si(OH)_2^{\bullet+}$ with H_2O, reaction 8a. [f] $SiO_3H_3^+$ produced from the reaction of $SiF(OH)_2^+$ with H_2O, reaction 3.

in reactions 1−3 observed in the low-pressure FT-ICR experiments[4] is reproduced under the higher pressures of the SIFT technique. Also, the trend in our measured rate coefficients of 1.6×10^{-9}, 1.1×10^{-9}, and 0.85×10^{-9} cm^3 molecule^{-1} s^{-1} for reactions 1−3, respectively, agrees with the trend in the FT-ICR values of 1.7×10^{-9}, 1.5×10^{-9}, and 1.4×10^{-9} cm^3 molecule^{-1} s^{-1},[4] although our results show a sharper decline in rate.

The terminal ion in the reaction sequence 1−3 was observed to become hydrated under the SIFT operating conditions with at least two molecules of water in reactions of type (11) with n

$$Si(OH)_3(H_2O)_n^+ + H_2O \rightarrow Si(OH)_3(H_2O)_{n+1}^+ \quad (11)$$

$= 0$ and 1. There was evidence also for the formation of the third hydrate at high flows of water vapor. Only the first hydration was observed at the much lower pressures of the FT-ICR experiments[4] and with an effective bimolecular rate coefficient, $k = 3 \times 10^{-11}$ cm^3 molecule^{-1} s^{-1}, much smaller than either of the two values, $k = 1.0 \times 10^{-10}$ and 7.7×10^{-10} cm^3 molecule^{-1} s^{-1} (reported in Table 2), measured under SIFT conditions. A smaller FT-ICR value is expected if hydration occurs by termolecular collisional stabilization because of the much lower ambient pressure in the FT-ICR experiments. Also, radiative stabilization cannot be ruled out in the FT-ICR experiments. The two different values reported in Table 2 for the hydration of $Si(OH)_3^+$ correspond to two different modes of production of $Si(OH)_3^+$. The lower value, $k = 1.0 \times 10^{-10}$ cm^3 molecule^{-1} s^{-1}, was obtained when $Si(OH)_3^+$ was produced by reaction 8a, while the higher value, $k = 7.7 \times 10^{-10}$ cm^3 molecule^{-1} s^{-1}, was obtained when $Si(OH)_3^+$ was produced by reaction 3. Our calculations show that reaction 8a is considerably more exothermic than reaction 3, by 22.9 vs 1.5 kcal mol^{-1}, which means that the $Si(OH)_3^+$ produced by reaction 8a is likely to contain substantially more internal energy upon its initial formation. If the collisional deactivation of this excited ion is incomplete prior to its subsequent addition to water, a lower

TABLE 3: Total Energies (hartrees) and Zero-Point Energies (kcal mol^{-1}) for Selected Closed-Shell Molecules

molecule	HF/3-21G	B-LYP/6-31G(d,p)	ZPE[a]
H_2O, **1**	−75.585 96	−76.398 88	12.9
HF, **2**	−99.460 22	−100.411 48	5.6
SiF^+, **3**	−386.042 65	−389.021 18	1.4
$FSiOH_2^+$, **4**	−461.733 70	−465.493 58	16.6
TS **4**→**6**, **5**	−461.684 88	−465.448 79	14.0
$HOSi^+\cdots FH$, **6**	−461.700 26	−465.461 89	15.2
$SiOH^+$, **7**	−362.199 88	−365.016 32	7.3
SiF_3^+, **15**	−583.895 98	−588.773 09	5.8
$F_3SiOH_2^+$, **16**	−659.661 84	−665.290 00	21.1
TS **16**→**18**,**17**	−659.597 64	−665.236 58	18.9
$F_2(HO)Si^+\cdots FH$, **18**	−659.616 27	−665.248 48	19.9
$F_2(HO)Si^+$, **19**	−560.058 59	−564.770 71	12.5
$F_2Si(OH)(H_2O)^+$, **20**	−635.805 40	−641.273 24	28.2
TS **20**→**22**, **21**	−635.742 63	−641.222 52	25.8
$F(HO)HOSi^+\cdots FH$, **22**	−635.754 92	−641.232 02	26.9
$FSi(OH)_2^+$, **23**	−536.210 21	−540.763 53	19.3
$FSi(OH)_2(H_2O)^+$, **24**	−611.939 32	−617.252 09	35.0
TS **24**→**26**, **25**	−611.877 71	−617.201 03	32.3
$(HO)_2Si^+\cdots FH$, **26**	−611.885 11	−617.208 31	33.4
$Si(OH)_3^+$, **27**	−512.352 03	−516.752 65	26.2
$Si(OH)_3(H_2O)^+$, **28**	−588.063 53	−593.227 07	42.0
$Si(OH)_3(H_2O)_2^+$, **29**	−663.719 50	−669.675 97	56.8

[a] From B-LYP/6-31G(d,p) harmonic frequency calculations; unscaled.

rate coefficient is likely to result. An alternative explanation might be sought in the formation of different isomers of $Si(OH)_3^+$, but our calculations indicate that the formation of the higher-energy isomer $OSi^+(OH)OH_2$ (which is 42 kcal mol^{-1} higher in energy than $Si(OH)_3^+$) would be endothermic, even for reaction 8a. Finally, we note that our experiments also indicated some small production of $SiF_2OH_2^{\bullet+}$ (ca. 10%) by F-atom elimination in the primary reaction of SiF_3^+ with H_2O (after correction for the 29 isotope of Si in SiF_3^+, which was not sufficiently resolved from the 28 isotope by the upstream quadrupole). This ion appeared to initiate the sequential HF-elimination reactions 12 and 13 followed by the hydration reaction 10. Production of $SiF_2OH_2^{\bullet+}$ from ground-state SiF_3^+ and H_2O by F-atom elimination was computed in this study to be endothermic by 38.9 kcal mol^{-1} at ROHF/6-31G(d,p), which implies internal excitation of a small fraction of the SiF_3^+ extracted from the ion source.

$$SiF_2OH_2^{\bullet+} + H_2O \rightarrow SiF(OH)(H_2O)^{\bullet+} + HF \quad (12)$$

$$SiF(OH)(H_2O)^{\bullet+} + H_2O \rightarrow Si(OH)_2(H_2O)^{\bullet+} + HF \quad (13)$$

Structures and Energetics. Molecular orbital calculations were performed in order to gain insight into the structures and energies of the ions observed experimentally, as well as plausible intermediates and transition states. Total electronic energies for all species investigated are shown in Tables 3 and 4. Relative energies are given in Tables 5−7. Optimized geometries are displayed in Figures 4−6.

Double-Well Potential-Energy Surfaces. Figure 7 displays the critical points calculated for the potential-energy surface associated with the reaction of SiF^+ with H_2O, reaction 5. It can be seen that the overall reaction can be represented by a double-well potential involving three sequential elementary processes: (1) formation of a hydrated complex, reaction 14;

$$SiF^+ + H_2O \rightarrow SiF^+\cdots OH_2 \quad (14)$$

(2) an intramolecular H-atom transfer, viz., a 1,3-H-atom shift,

TABLE 4: Total Energies (hartrees) and Zero-Point Energies (kcal mol^{-1}) for Selected Open-Shell Molecules and Water

molecule	ROHF/3-21G	ROHF/6-31G(d,p)	ZPE[a]
H_2O, **1**[b]	−75.585 96	−76.023 62	13.0
$F^{\bullet}$, **8**	−98.844 65	−99.361 79	
$SiF_2^{\bullet+}$, **9**	−484.924 43	−487.529 13	3.3
$F_2SiOH_2^{\bullet+}$, **10**	−560.654 24	−563.656 04	18.7
TS **10**→**10B**, **10A**	−563.584 59		16.1
$F(OH)Si^+\cdots FH$, **10B**	−560.610 53	−563.612 54	17.1
$FSiOH^{\bullet+}$, **11**	−461.078 92	−463.554 50	9.8
$FSiOH(H_2O)^{\bullet+}$, **12**	−536.790 20	−539.667 15	25.5
TS **12**→**12B**, **12A**		−539.595 86	22.6
$(HO)_2Si^+\cdots FH$, **12B**	−535.742 61	−539.623 98	24.0
$Si(OH)_2^{\bullet+}$, **13**	−437.223 11	−439.575 37	16.6
$Si(OH)_2(H_2O)^{\bullet+}$, **14**	−512.917 94	−515.673 55	36.3

[a] From ROHF/6-31G(d,p) harmonic frequency calculations; scaled by 0.89. [b] Total electronic and zero-point vibrational energies for H_2O are reported for RHF, rather than ROHF, calculations, with the same basis sets as specified for other species.

TABLE 5: Relative Energies[a] of Critical Points on the Potential-Energy Surfaces Associated with the HF-Elimination Reactions of SiF^+, SiF_3^+, SiF_2OH^+, and $SiF(OH)_2^+$ with H_2O

reaction	reactants	adduct	TS[b]	product ion solvated by HF	separated products
$SiF^+ + H_2O \rightarrow SiOH^+ + HF$	+ 43.8	0.0	+ 25.5	+ 18.5	+ 37.6
$SiF_3^+ + H_2O \rightarrow SiF_2OH^+ + HF$	+ 71.7	0.0	+ 31.3	+ 24.9	+ 64.7
$SiF_2OH^+ + H_2O \rightarrow SiF(OH)_2^+ + HF$	+ 62.2	0.0	+ 29.4	+ 24.6	+ 58.3
$SiF(OH)_2^+ + H_2O \rightarrow Si(OH)_3^+ + HF$	+ 53.5	0.0	+ 29.3	+ 25.9	+ 52.0

[a] In kilocalories per mole, from B-LYP/6-31G(d,p) optimizations; unscaled ZPE included. [b] Energy of the transition state between the adduct and product ion solvated by HF.

forming a second solvated cluster, reaction 15;

$$SiF^+\cdots OH_2 \rightarrow HF\cdots SiOH^+ \quad (15)$$

and (3) dissociation of the second cluster into products, reaction 16.

$$HF\cdots SiOH^+ \rightarrow HF + SiOH^+ \quad (16)$$

The first well depth along the reaction coordinate corresponds to the stabilization energy of the first solvated cluster, $SiF^+\cdots OH_2$, relative to the energy of the reactants, while the second well depth corresponds to the stabilization energy of the second solvated cluster, $HF\cdots SiOH^+$, relative to the energy of the products. Neither $SiF^+\cdots OH_2$ nor $HF\cdots SiOH^+$ was observed experimentally, presumably due to insufficient time for the collisional stabilization of the short-lived complex into either of the two potential energy wells. An examination of the topology of the potential-energy surface in Figure 7 is instructive in terms of understanding the reason for the occurrence of reaction 5: not only is the overall reaction exothermic (by 6.2 kcal mol^{-1}) but also the energy of the transition structure for the isomerization of the initial adduct ion to the solvated ion lies below that of both reactants and products.

Topological features similar to those of the $SiFOH_2^+$ potential-energy surface for reaction 5 apply to the potential-energy surfaces for reactions 1−3. Table 5 summarizes the relative energies of the important features on these surfaces. The exothermicity for HF-elimination drops for the reaction sequence 1−3. The exothermicities for reactions 1−3 calculated at B-LYP/6-31G(d,p) are −7.0, −3.9, and −1.5 kcal mol^{-1} (unscaled zero-point vibrational energies), respectively. Also,

TABLE 6: Total Electronic Energies[a] and Relative Energies[b] of Reactants and Products Associated with the Reactions of $SiF_2^{\bullet+}$ with H_2O

reaction	E(reactants)[a]	E(products)[a]	ΔE[b]
$SiF_2^{\bullet+} + H_2O \rightarrow SiFOH^{\bullet+} + HF$	−563.552 75	−563.566 19	−9.2
$SiFOH^{\bullet+} + H_2O \rightarrow Si(OH)_2^{\bullet+} + HF$	−539.578 12	−578.587 06	−6.1
$Si(OH)_2^{\bullet+} + H_2O \rightarrow Si(OH)_3^+ + H^\bullet$ (90%)	−515.598 99	−515.629 98	−22.9
$\rightarrow Si(OH)_2(H_2O)^{\bullet+}$ (10%)	−515.598 99	−515.673 55	−40.0
$Si(OH)_3^+ + H_2O \rightarrow Si(OH)_3(H_2O)^+$	−593.151 53[c]	−593.227 07[c]	−44.5[d]
$Si(OH)_3(H_2O)^+ + H_2O \rightarrow Si(OH)_3(H_2O)_2^+$	−669.635 95[c]	−669.675 97[c]	−29.5[d]

[a] In hartrees, from ROHF/6-31G(d,p) optimizations; zero-point vibrational energy (ZPE) not included. [b] In kilocalories per mole, from ROHF/6-31G(d,p) optimizations; ZPE included, scaled by 0.89.[66] [c] In hartrees, from B-LYP/6-31G(d,p) optimizations; ZPE not included. [d] In kilocalories per mole, from B-LYP/6-31G(d,p) optimizations; unscaled ZPE included.

TABLE 7: Total Electronic and Relative Energies of Reactants and Transition States Associated with the HF-Elimination Reactions of Reactions of $SiF_2^{\bullet+}$ and $SiFOH^{\bullet+}$ with H_2O

ROHF/6-31G(d,p)[a]

reaction	E(reactants)[b]	ZPE[c]	E(TS)[b]	ZPE[c]	ΔE[d]
$SiF_2^{\bullet+} + H_2O \rightarrow SiFOH^{\bullet+} + HF$	−563.552 75	16.2	−563.584 59	16.1	−20.1
$SiFOH^{\bullet+} + H_2O \rightarrow SiF(OH)_2^{\bullet+} + HF$	−539.578 11	22.8	−539.595 86	22.6	−11.3

UB-LYP/6-31G(d,p)[a]

reaction	E(reactants)[b]	ZPE[f]	E(TS)[b]	ZPE[f]	ΔE[g]
$SiF_2^{\bullet+} + H_2O \rightarrow SiFOH^{\bullet+} + HF$	−565.247 72	16.1	−565.295 48	16.1	−30.0
$SiFOH^{\bullet+} + H_2O \rightarrow SiF(OH)_2^{\bullet+} + HF$	−541.245 26	22.7	−541.280 87	22.9	−22.1

[a] Total electronic and zero-point (ZPE) energy for H_2O is included at RHF/6-31G(d,p). [b] In hartrees; ZPE not included. [c] In kilocalories per mole, from optimized ROHF/6-31G(d,p) (open-shell) and RHF/6-31G(d,p) (closed-shell) structures; scaled by 0.89. [d] In kilocalories per mole; scaled ZPE included. [e] Total electronic and ZPE for H_2O is included at RB-LYP/6-31G(d,p). [f] In kilocalories per mole, from optimized UB-LYP/6-31G(d,p) (open-shell) and RB-LYP/6-31G(d,p) (closed-shell) structures; unscaled. [g] In kilocalories per mole; unscaled ZPE included.

the difference in energy between the initial reagents and the transition state for reactions 1−3 decreases from 40.4 to 32.8 to 24.2 kcal mol^{-1}, respectively. This trend parallels the trend observed in the magnitude of the rate coefficients measured for reactions 1−3 which have values of 1.6×10^{-9}, 1.1×10^{-9}, and 0.85×10^{-9} cm^3 $molecule^{-1}$ s^{-1}, respectively.

At first glance the trend in the exothermicity of reactions 1−3 may be surprising given that these reactions all involve the same reactant and product neutrals, the rupture of a Si−F bond, and the formation of a Si−OH bond. However, a close inspection of the computed geometries in Figure 4 reveals a change in the length of the Si−F bond being broken (1.560, 1.565, and 1.568 Å, respectively) and a change in the length of the Si−OH bond being formed (1.583, 1.593, and 1.598 Å, respectively). Clearly, there is a monotonic lengthening of both Si−F and Si−OH bonds in going from reactions 1−3. This suggests a decrease in the conjugative stabilization of the product ions vis-à-vis that of reactant ions and therefore a decrease in exothermicity.

The exothermicities of the two sequential HF-elimination reactions initiated by the radical cation $SiF_2^{\bullet+}$ are similar to those of the closed-shell ions SiF^+ and SiF_3^+ (see Tables 5 and 6), and these reactions also appear to proceed via an intramolecular H-atom transfer analagous to reactions 14−16. The first of these HF-elimination reactions is exothermic by 9.2 kcal mol^{-1} as calculated at ROHF/6-31G(d,p); the second is exothermic by 6.1 kcal mol^{-1} at the same level of theory. Higher-level calculations at UB-LYP/6-31G(d,p) were performed only for the reactants and transition structures of these open-shell systems (see Table 7) and this was done to explore further the correlation of reactivity with energetics.

Correlation of Reactivity with Energetics. The double-minima potential-energy surfaces computed for the six HF-elimination/intramolecular H-atom transfer reactions observed in our experiments are reminiscent of those proposed for gas-phase S_N2 reactions for which the reaction efficiency has been shown to correlate with the energy defect between reactants and the transition state.[20,21] RRKM calculations by Braumann and collaborators have demonstrated that even though the transition state for such reactions may lie substantially below the potential energy of the reactants, a significantly reduced reaction efficiency can result.[20] As can be seen from Figure 8, this also appears to be the case for the six HF-elimination reactions investigated in this study. The energy defect between reactants and the transition state, ΔE, computed for the six reaction ranges from −18.3 to −40.4 kcal mol^{-1}, while reaction efficiences span values between 0.030 and 0.70. A fairly smooth increase in reaction efficiency with increasing energy defect is observed with the four even-electron systems, viz., reactions 1−3 and 5. However, the correlation appears to fail for the two odd-electron reactions 6 and 7: the measured reaction efficiencies for these two reactions are the same, even though the computed energy defect differs by 7.9 kcal mol^{-1}.

Hydrated Ions. Several hydration reactions have been observed in our experiments. Specifically, the ions $Si(OH)_2^{\bullet+}$, $Si(OH)_3^+$, and $Si(OH)_3(H_2O)^+$ have all been observed to hydrate under SIFT conditions, presumably by termolecular association. Geometric parameters computed for the hydrated ions are given in Figure 6 in structures **14**, **28**, and **29**, respectively.

The preferred reaction of the terminal $Si(OH)_2^+$ ion in the HF-elimination sequence initiated by SiF_2^+ and H_2O to produce $Si(OH)_3^+$ rather than to add water is not surprising, given the substantial exothermicity of this bimolecular channel. However, at the moderate helium pressure of the SIFT experiments, stabilization of the $Si(OH)_2(H_2O)^+$ hydrate, likely to have structure **14**, is also observed and so competes with HF-elimination. The calculations indicate the formation of a relatively strong $Si-OH_2$ bond, 40.0 kcal mol^{-1}, upon hydration.

Our experiments have shown that $Si(OH)_3^+$, ion **27**, reacts further with H_2O to form an adduct ion in which, according to our computations, the central silicon atom exists in a nearly tetrahedral bonding arrangement, ion **28**. Again, a relatively strong $Si-OH_2$ bond, in this case 44.5 kcal mol^{-1}, is formed. Examination of the optimized structure of ion **28** reveals the existence of three nearly equivalent Si−OH bonds (in which the bond lengths vary only on the order of 0.001 Å) and of one $Si-OH_2$ bond which is considerably longer (1.783 Å). The greater length of the Si^+-OH_2 distance is attributed to an electrostatic repulsion between the partial positive charge on the oxygen, formed by coordination to Si^+, and the remaining large positive charge on silicon. Such a repulsion results in an

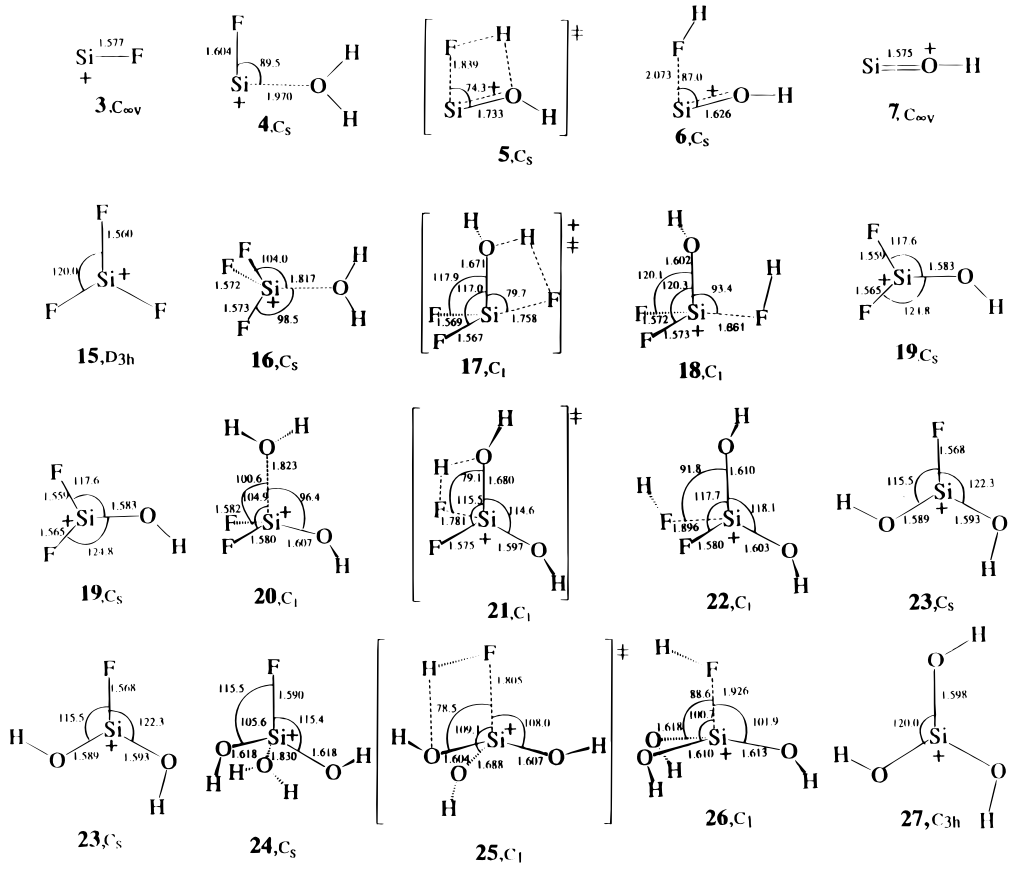

Figure 4. Geometric parameters for reactant ions, intermediates, transition states, and product ions associated with the reactions of SiF^+, SiF_3^+, SiF_2OH^+, and $SiF(OH)_2^+$ with H_2O. Bond lengths and bond angles are given only for heavy (non-hydrogen) atoms.

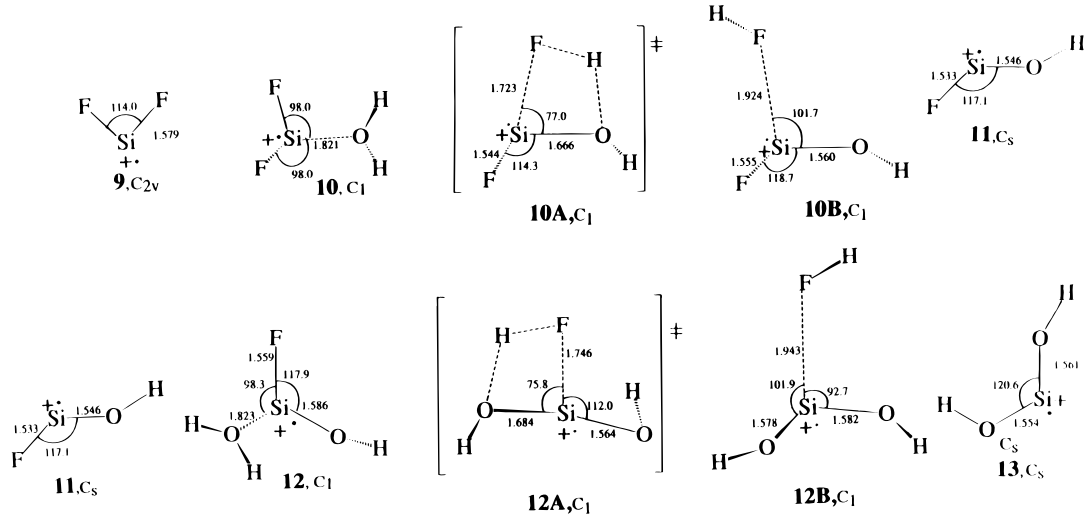

Figure 5. Geometric parameters for reactant ions, intermediates, transition states, and product ions associated with the reactions $SiF_2^{\bullet+}$ and $SiFOH^{\bullet+}$ with H_2O. Bond lengths and bond angles are given only for heavy (non-hydrogen) atoms.

elongation of the Si−OH_2 distance compared to those of the three Si−OH bonds in **29**, in which such interactions are not present.

Calculations of structural isomers associated with the empirical formula $SiO_5H_7^+$ gave structure **29** to be at the global minimum. In this structure the central silicon atom remains in a nearly tetrahedral bonding arrangement but with one of the Si−OH bonds considerably longer than the other three. The oxygen associated with this bond is attached to *two* hydrogen atoms, with one O−H being the characteristic length (0.965 Å) while the other is very long (1.289 Å). The proton involved in

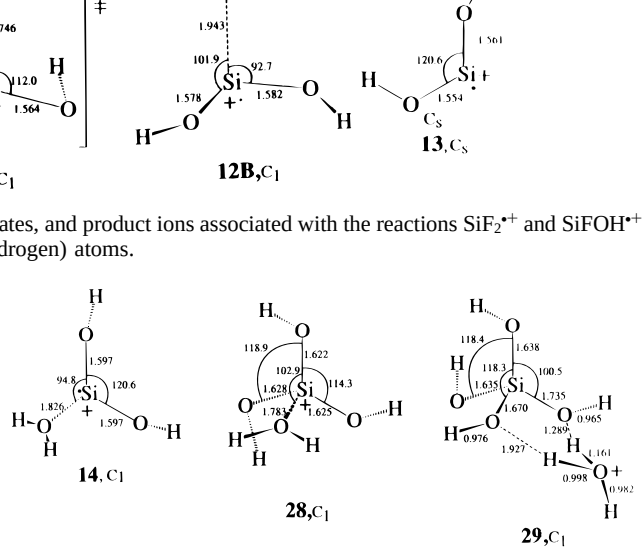

Figure 6. Geometric parameters computed for monohydrated $Si(OH)_2^{\bullet+}$, $Si(OH)_3^+$, and $Si(OH)_3(H_2O)^+$.

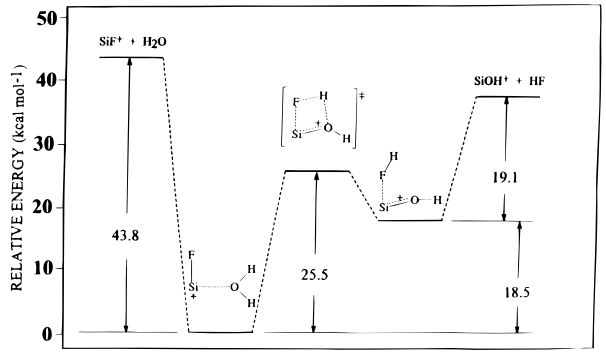

Figure 7. Potential energy hypersurface associated with the gas-phase ion−molecule reaction of SiF^+ with H_2O. The topology of this surface is analogous to those associated with the HF elimination reactions of SiF_3^+, SiF_2OH^+, $SiF(OH)_2^+$, $SiF_2^{\bullet+}$ and $SiF(OH)^{\bullet+}$ with H_2O.

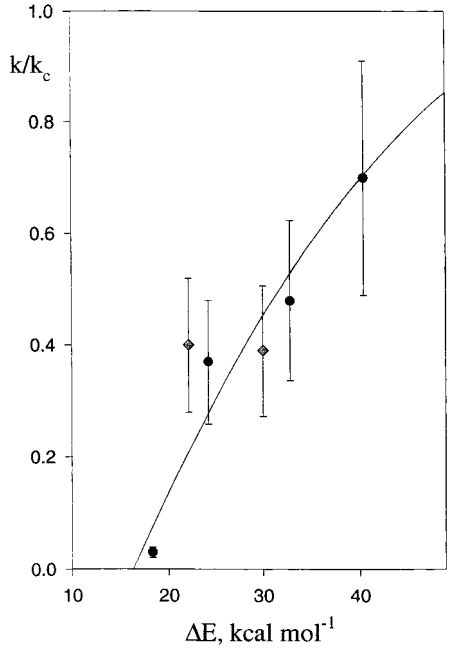

Figure 8. Correlation of HF-elimination efficiency with the energy defect between the reactants and the transition state. Closed circles represent the HF-elimination reactions initiated by the even-electron ions SiF^+ and SiF_3^+, and the shaded squares represent HF-elimination reactions initiated by the odd-electron ion $SiF_2^{\bullet+}$. A polynomial rather than a linear fit was chosen to better describe the trend in the data.

the latter bond is more firmly attached to the solvating molecule (O−H distance, 1.161 Å), and **29** may then be regarded more properly as a nearly tetrahedral $Si(OH)_4$ molecule which solvates a hydronium ion rather than protonated $Si(OH)_4H^+$ solvated by a water molecule.

Conclusions

Eliminations of hydrogen fluoride have been shown to predominate under SIFT conditions in the reactions of SiF^+, SiF_2^+, $SiFOH^+$, SiF_3^+, SiF_2OH^+, and $SiF(OH)_2^+$ with H_2O in which all Si−F bonds present intially are replaced by Si−OH bonds. Measured rate coefficients are consistent with previous FT-ICR measurements at much lower pressures. Insight into the mechanism of these reactions has been provided by computations of structures and energies for reactant and product ions as well as possible transition states. The calculations show double minima in the potential-energy profiles. A key feature of the reaction mechanism in each case is intramolecular H-atom transfer. The magnitude of the rate coefficient for HF-elimination is controlled by the energy defect between the initial energy of the reactants and the energy of the transition state, increasing as the energy defect increases. Theory also has confirmed that all of the HF-elimination reactions involving ground-state reactants are exothermic and has shown that successive HF-eliminations decrease in their exothermicity, for both the sequences initiated by $SiF_2^{\bullet+}$ and by SiF_3^+.

Several hydrated $Si(OH)_2^{\bullet+}$ and $Si(OH)_3^+$ ions have been observed to be formed in higher-order reactions under SIFT conditions. Two types of bonding with H_2O have been characterized. The bonding with water in $Si(OH)_2(H_2O)^{\bullet+}$ and $Si(OH)_3(H_2O)^+$ involves relatively strong Si−O bonds. Molecular orbital calculations have shown that the lowest-energy isomer associated with the addition of two H_2O molecules to $Si(OH)_3^+$ has a structure best described as tetrahedral $Si(OH)_4$ solvating H_3O^+ through hydrogen bonding.

Acknowledgment. We thank Steve Quan and Alwin Cunje for technical assistance. Continued financial support from the Natural Sciences and Engineering Research Council of Canada is much appreciated.

References and Notes

(1) Streitwieser, A., Jr.; Heathcock, C. H. *Introduction to Organic Chemistry*, 3rd ed.; Macmillan Publishing: New York, 1985.

(2) See, for example: (a) Damm, W.; Dickhaut, J.; Wetterich, F.; Giese, B. *Tetrahedron Lett.* **1993,** *34*, 431. (b) Koch, W.; Holthausen, M. C. *Int. J. Mass Spectrom. Ion Processes* **1993**, *127*, 183. (c) Marshall, P. *Chem. Phys. Lett.* **1993**, *201*, 493. (d) Magnusson, B. *J. Am. Chem. Soc.* **1993**, *115*, 1051. (e) Guerra, M. *J. Am. Chem. Soc.* **1993**, *115*, 11926. (f) Earley, C. W. *J. Comput. Chem.* **1993**, *14*, 216. (g) De Almeida, W. B.; O'Malley, P. J. *J. Chem. Soc., Faraday Trans.* **1993**, *89*, 983. (h) Remko, M.; Liedl, K. R.; Rode, B. M. *J. Chem. Soc., Faraday Trans.* **1993**, *89*, 2375. (i) Lucas, D. J.; Curtiss, L. A.; Pople, J. A. *J. Chem. Phys.***1993**, *99*, 6697. (j) Ferrari, A. M.; Ugliengo, P.; Garrone, B. *J. Phys. Chem.* **1993**, *97*, 2671. (k) Boldyrev, A. I.; Simons, J. *J. Phys. Chem.* **1993**, *97*, 5875. (l) Luke, B. T. *J. Phys. Chem.* **1993**, *97*, 7505. (m) Gordon, M. S.; Damrauer, R.; Krempp, M. *J. Phys. Chem.* **1993**, *97*, 7820. (n) Darling, C. L.; Schlegel, H. B. *J. Phys. Chem.* **1993**, *97*, 8207. (o) A. Luna, A.; Yáñez, M. *J. Phys. Chem.* **1993**, *97*, 10659. (p) Pelminschikov, A. G.; Morosi, G.; Gamba, A.; Zecchina, A.; Bordiga, S.; Paukshtis, E. A. *J. Phys. Chem.* **1993**, *97*, 11979. (q) Politzer, P.; Seminario, J. M.; Concha, M. C.; Murray, J. S. *Theor. Chim. Acta* **1993**, *85*, 127. (r) Limtrakul, J. *J. Mol. Struct. (THEOCHEM)* **1993**, *107*, 105. (s) Fan, K.; Iwata, S. *Chem. Phys. Lett.* **1992**, *189*, 401. (t) Luna, A.; Mó, O.; Yáñez, M. *Chem. Phys. Lett.* **1992**, *197*, 581. (u) Jug, K.; Fasold, B. *Int. J. Quantum Chem.* **1992**, *41*, 687. (v) Tachibana, A.; Fueno, H.; Okazaki, I.; Yamabe, T. *Int. J. Quantum Chem.* **1992**, *42*, 929.

(3) See, for example: (a) Bohme, D. K. *Int. J. Mass Spectrom. Ion Processes* **1990**, *100*, 719. (b) Bohme, D. K. *Adv. Gas-Phase Ion Chem.* **1992**, *1*, 225. (c) Fahey, D. W.; Dotan, I.; Fehsenfeld, F. C.; Albritton, D. L.; Viehland, L. A. *J. Chem. Phys.* **1981**, *74*, 3320. (d) Anicich, V. G.; Bowers, M. J. *J. Am. Chem. Soc.* **1974**, *96*, 1279. (e) Srinivas, R.; Bohme, D. K.; Hrusàk, J.; Schröder, D.; Schwarz, H. *J. Am. Chem. Soc.* **1992**, *114*, 1939.

(4) Grandinetti, F.; Occhiucci, G.; Ursini, O.; de Petris, G.; Speranza, M. *Int. J. Mass Spectrom. Ion Processes* 1993, *124*, 21.

(5) Gaydon, A. D. *Dissociation Energies and Spectra of Diatomic Molecules*, 3rd ed.; Chapman and Hall: London, 1968.

(6) Kerr, J. A. *Chem. Rev.* **1966**, *66*, 465.

(7) Mackay, G. I.; Vlachos, G. D.; Bohme, D. K.; Schiff, H. I. *Int. J. Mass Spectrom. Ion Phys.* **1988**, *36*, 259.

(8) Raksit, A. B.; Bohme, D. K. *Int. J. Mass Spectrom. Ion Phys.* **1983**, *55*, 69.

(9) (a) Frisch, M. J.; Trucks, G. W.; Schlegel, H. B.; Gill, P. M. W.; Johnson, B. G.; Robb, M. A.; Cheeseman, J. R.; Keith, T.; Petersson, G. A.; Montgomery, J. A.; Raghavachari, K.; Al-Laham, M. A.; Zakrzewski, V. G.; Ortiz, J. V.; Foresman, J. B.; Cioslowski, J.; Stefanov, B. B.; Nanayakkara, A.; Challacombe, M.; Peng, C. Y.; Ayala, P. Y.; Chen, W.; Wong, M. W.; Andres, J. L.; Replogle, B. S.; Gomperts, R.; Martin, R. L.; Fox, D. J.; Binkley, J. S.; Defrees, D. J.; Baker, J.; Stewart, J. P.; Head-Gordon, M.; Gonzalez, C.; Pople, J. A. *GAUSSIAN 94*, Revision B.2; Gaussian, Inc.: Pittsburgh, PA, 1995. (b) Frisch, M. J.; Trucks, G. W.; Schlegel, H. B.; Gill, P. M. W.; Johnson, B. G.; Wong, M. W.; Foresman, J. B.; Robb, M. A.; Head-Gordon, M.; Replogle, B. S.; Gomperts, R.; Andres, J. L.; Raghavachari, K.; Binkley, J. S.; Gonzalez, C.; Martin, R.

L.; Fox, D. J.; Defrees, D. J.; Baker, J.; Stewart, J. J. P.; Pople, J. A. *GAUSSIAN 92/DFT*, Revision F.4; Gaussian, Inc.: Pittsburgh, PA, 1993.

(10) (a) Binkley, J. S.; Pople, J. A.; Hehre, W. J. *J. Am. Chem. Soc.* **1980**, *102*, 939. (b) Gordon, M. S.; Binkley, J. S.; Pople, J. A.; Pietro, W. J.; Hehre, W. J. *J. Am. Chem. Soc.* **1982**, *104*, 2797. (c) Pietro, W. J.; Francl, M. M.; Hehre, W. J.; Defrees, D. J.; Pople, J. A.; Binkley, J. S. *J. Am. Chem. Soc.* **1982**, *104*, 5039.

(11) See, for example: (a) Parr, R. G.; Yang, W. *Density Functional Theory of Atoms and Molecules*; Oxford University Press: Oxford, U.K., 1989. (b) Labanowski, J. K., Andzelm, J. W., Eds.; *Density Functional Methods in Chemistry*; Springer-Verlag: New York, 1991. (c) Perdew, J. P.; Chevary, J. A.; Vosko, S. H.; Jackson, K. A.; Pederson, M. R.; Singh, D. J.; Fiolhais, C. *Phys. Rev. B* **1992**, *46*, 6671. (d) Andzelm, J.; Wimmer, B. *J. Chem. Phys.* **1992**, *96*, 1280. (e) Scuseria, G. B. *J. Chem. Phys.* **1992**, *97*, 7528. (f) Becke, A. D. *J. Chem. Phys.* **1992**, *97*, 9173. (g) Sosa, C.; Lee, C. *J. Chem. Phys.* **1993**, *98*, 8004. (h) Stephens, P. J.; Devlin, F. J.; Ashwar, C. S.; Chabalowski, C. F.; Frisch, M. J. *Faraday Dissuss.* **1994**, *99*, 103.

(12) Slater, J. C. The Self-Consistent Field for Molecular and Solids. *Quantum Theory of Molecular and Solids;* McGraw-Hill: New York, 1974; Vol. 4.

(13) Becke, A. D. *Phys. Rev. A* **1988**, *38*, 3098.

(14) (a) Lee, C.; Yang, W.; Parr, R. G. *Phys. Rev. B* **1988**, *37*, 785. (b) Miehlich, B.; Savin, A.; Stoll, H.; Preuss, H. *Chem. Phys. Lett.* **1989**, *157*, 200.

(15) (a) Hehre, W. J.; Ditchfield, R.; Pople, J. A. *J. Chem. Phys.* **1972**, *56*, 2257. (b) Hariharan, P. C.; Pople, J. A. *Chem. Phys. Lett.* **1972**, *16*, 217. (c) Hariharan, P. C.; Pople, J. A. *Theor. Chim. Acta* **1973**, *28*, 213. (d) Francl, M. M.; Pietro, W. J.; Hehre, W. J.; Binkley, J. S.; Gordon, M. S.; Defrees, D. J.; Pople, J. A. *J. Chem. Phys.* **1982**, *77*, 3654. (e) Frisch, M. J.; Pople, J. A.; Binkley, J. S. *J. Chem. Phys.* **1984**, *80*, 3265.

(16) (a) Baker, J. *J. Comput. Chem.* **1986**, *7*, 385. (b) Baker, J. *J. Comput. Chem.* **1987**, *8*, 563. (c) Simons, J.; Jorgensen, P.; Miller, W. H.; Ozment, J. *J. Phys. Chem.* **1983**, *87*, 2745. (d) Cerjan, C. J.; Miller, W. H. *J. Chem. Phys.* **1981**, *75*, 2800.

(17) Peng, C.; Schlegel, H. B. *Isr. J. Chem.* **1993**, *33*, 449.

(18) Gonzalez, C.; Schlegel, H. B. *J. Chem. Phys.* **1989**, *90*, 2154.

(19) McWeeny, R.; Diercksen, G. *J. Chem. Phys.* **1968**, *49*, 4852.

(20) Olmstead, W. N.; Braumann, J. L. *J. Am. Chem. Soc.* **1977**, *99*, 4219.

(21) Pellerite, M. J.; Brauman, J. L. *J. Am. Chem. Soc.* **1980**, *102*, 5994.

(22) Su, T.; Chesnavich, W. J. *J. Chem. Phys.* **1982**, *76*, 5183.